Building Lunar Maps for Terrain Relative Navigation and Hazard Detection Applications

Carolina I. Restrepo[1], Noah E. Petro[2], Michael K. Barker[3], Erwan Mazarico[4], Andrew Liounis[5], Christopher Gnam[6], Stephen Scheidt[7], Jacob Richardson[8]
NASA Goddard Space Flight Center, Greenbelt, MD

Adnan I. Ansar[9], Yang Cheng[10], Zachary Morgan[11], Yumi Iwashita[12]
Jet Propulsion Laboratory, California Institute of Technology, Pasadena, CA

Ross A. Beyer[13]
SETI Institute, Mountain View, CA and NASA Ames Research Center, Moffett Field, CA

Terrain Relative Navigation (TRN) systems localize a spacecraft with respect to a map of the surface by comparing descent imagery to that reference map. The spacecraft position estimates can only be as accurate as the reference map itself. Accurate map products that are based on orbital reconnaissance data must be validated for navigation applications to ensure that all relevant error sources are minimized. Currently available map products have been generated for scientific applications, so the need for accurate TRN maps remains a gap to be filled for upcoming lunar lander missions, in particular missions to the South Pole region. Additionally, representative high-resolution maps that contain lander-scale features are needed for successful development and testing of Hazard Detection (HD) systems. This paper describes one of NASA's current efforts to develop benchmark data sets that can be used for developing and testing TRN and HD algorithms as well as suggested processes and metrics for generating and validating lunar maps that can be used for navigation and hazard detection.

[1] Aerospace Engineer, Navigation and Mission Design Branch, AIAA Senior Member.
[2] Chief, Planetary Geology, Geophysics and Geochemistry Laboratory.
[3] Space Research Scientist, Planetary Geology, Geophysics and Geochemistry Laboratory.
[4] Space Research Scientist, Planetary Geology, Geophysics and Geochemistry Laboratory.
[5] Aerospace Engineer, Navigation and Mission Design Branch.
[6] Aerospace Engineer, Navigation and Mission Design Branch.
[7] Space Research Scientist, Planetary Geology, Geophysics and Geochemistry Laboratory.
[8] Space Research Scientist, Planetary Geology, Geophysics and Geochemistry Laboratory.
[9] Group Supervisor, Mobility and Robotic Systems Section.
[10] Robotics Technologist, Mobility and Robotic Systems Section.
[11] Data Scientist, Instrument Software and Science Data Systems.
[12] Robotics Technologist, Mobility and Robotic Systems Section.
[13] Senior Research Scientist, SETI Institute

I. Introduction

NASA and its partners have been steadily investing in the development of Terrain Relative Navigation (TRN) and Hazard Detection (HD) systems including sensor hardware, guidance, navigation, and control algorithms, and new flight processors that can support onboard image processing in real-time [1]. An additional key piece to the successful development and performance of TRN and HD systems is the availability of high-quality reference maps of the lunar surface. While there is an abundance of lunar data suitable for science applications, the process of building large enough maps for TRN applications results in production artifacts that arise from merging different sources of orbital imagery and topography data. Due to the difference in coverage and resolution of the various data sources, producing a seamless flight-ready TRN map is a tedious process. Currently, for a given site and a given TRN system, it is necessary to manually search for all the applicable imagery and topographic data from multiple sources, go through multiple iterations of map products to identify and minimize potential errors, and use dedicated software tools to merge the data. Additionally, validating the resulting map products is a non-trivial task.

Two recent examples of flight TRN systems are the Mars2020 Lander Vision System [2] and the OSIRIS-REx Natural Feature Tracking algorithm [3], both of which navigated their respective spacecraft to a sample collection site. Each of these missions approached the problem of map generation and validation in different ways, but accurate maps with well-understood sources of error were key in the success of both. While there are valuable and applicable lessons learned from the Mars2020 and the OSIRIS-REx missions' successes, the Moon, and in particular, the South pole region brings a unique set of challenges. Unlike previous missions, the process for building and validating maps for the Moon will need to be repeated for each landing site so it is necessary to develop standards and metrics that can be applicable to multiple sites and various TRN systems to the extent possible.

To address the current need for improved accuracy and coverage of lunar surface maps, NASA is funding a new project called Lunar Navigation Maps (LuNaMaps). Leveraging the experience from the Mars2020 and the OSIRIS-REx navigation teams as well as the expertise from the Lunar Reconnaissance Orbiter (LRO) instrument scientists, we aim to develop methodical processes to improve the quality of lunar maps, identify and quantify potential sources of error, and optimally combine available data sources and software tools to build map products suitable for Entry, Descent, and Landing systems. In addition to software tools and guidelines for building map products, the LuNaMaps project has the goal of producing a set of benchmark data sets for both TRN and HD that will be shared with the community as examples of validated map products.

This paper describes the current project plans as well as some preliminary results. Section II is a brief summary of the three main sources of lunar data, LRO Laser Altimeter (LOLA), LRO Narrow Angle Camera (LROC NAC), and the Kaguya Terrain Camera (TC). Section III describes the planned process for building TRN map products along with some preliminary results on eliminating potential sources of error. Section IV outlines the process for generating benchmark data sets for HD applications. Sections V and VI outline the current plans for map validation and TRN performance evaluation respectively.

II. Lunar Data Sources

Lunar map products for TRN are derived from orbital data from the LRO instruments, LOLA and LRO Camera (LROC), as well as the Kaguya TC and other sources of imagery as they become available. Any data products used as a basis for TRN work should be rooted in appropriate foundational data products [4] which have rigorous spatial error and reporting.

A. LOLA

The LOLA instrument onboard LRO has collected nearly 7 billion globally-distributed measurements of surface height with a vertical precision of ~10 cm and an accuracy of ~1 m [5]. The LOLA dataset is used by the community as the geodetic framework, or "backbone", for aligning datasets from LRO and other lunar missions. LOLA is a time-of-flight laser altimeter operating with a firing rate of 28 Hz and a cross-shaped, 5-spot footprint on the surface canted by 26° from the along-track direction to optimize coverage overlap [6]. From commissioning in July 2009 to the start of the mapping phase in September 2009, LRO orbited in a 30 × 200 km elliptical orbit with periselene in the southern

hemisphere. Subsequently, LRO entered its nominal 50-km near-circular mapping orbit, where it remained until December 2011 when it transitioned to a near-frozen elliptical orbit similar to commissioning. After this time, LOLA collected very few returns in the northern hemisphere as the spacecraft was too high for altimetric ranging. From an altitude of 50 km, the cross-track spacing between each profile is 12 m with an along-track spacing of 57 m between each measurement in a profile, and each spot footprint has a diameter of 5 m, suggesting a natural minimum pixel scale of 5 m/pix for the LDEM product, the one we use here. The range precision inherent to the LOLA timing electronics is ~10 cm, which sets an absolute floor to the vertical geolocation uncertainty of any individual laser return.

B. LROC NAC

The LROC Narrow Angle Camera (NAC) are a pair of cameras capable of cm-scale per pixel images of the illuminated surface [7]. From a nominal 50 km orbit, the resolution of the camera is ~50 cm per pixel, generating images useful for the identification of surface features such as rocks and boulders. For the two years of the LRO primary science mission, LRO operated at the 50 km altitude generating observations of the lunar surface at the 50 cm/pix resolution scale. For polar areas, due to the low-light levels from the grazing low Sun angles, images are summed to improve signal-to-noise ratios, resulting in a ~2x lower spatial resolution than the nominal image scale. In addition to high-resolution images, multiple images of the same terrain under slightly different viewing geometries, typically acquired on back-to-back orbits of the LRO spacecraft enable stereo images which are used to generate digital elevation models DEMs [8]. These DEMs, tied to the LOLA base, are available at a 2 m/pix. Currently a number of DEMs have been generated by the LROC team that can be found at https://wms.lroc.asu.edu/lroc/rdr_product_select, as well as many more stereo observations that could be turned into DEMs. The DEMs do not, by the nature of how they are collected, provide any topographic detail of areas in shadow (or permanent shadow).

C. Kaguya TC

Kaguya TC on the SELenological and ENgineering Explorer "KAGUYA" (SELENE) collected stereo-pair data of the day-time side of the Moon from November 2007 to June 2009. Kaguya TC consists of two one-dimensional telescopes that collected images by a push-broom scanning approach. Image resolution is 10 m/pix, obtained from Kaguya's nominal altitude of 100 km. Each telescope has 4096 pixels, and TC acquired data with a nominal 3504 pixels (occasionally it was 4096 or 1752 pixels). TC has three observation modes: (i) a stereoscopic observation mode at high solar elevation angles, (ii) a monoscopic observation mode at lower solar elevation angle, and (iii) Spectral Profiler (SP) support observation mode. During the mission period Kaguya TC covered more than 99% of the lunar surface in stereo [9]. The JAXA team released several processed data sets, such as L2B and DTM. L2B is the image data obtained after dark and flat image calibrations of L2A raw data. DTM is the digital terrain model from L2B.

III. Terrain Relative Navigation Map Products

During the terminal stage of landing, a TRN system compares descent images to an onboard reference map for lander localization. Here, a map is defined as a georeferenced product (i.e. images of the surface or topographic data) and a DEM, or Digital Elevation Model, is defined as a 3-dimensional map of the surface. The onboard maps that a spacecraft carries must match the reality of the day of flight as close as possible. To localize the lander accurately, it is necessary that the reference map have as little geometric and photometric error as possible. Photometrically, it should resemble as closely as possible the real descent images to allow easy and reliable terrain matching. Geometrically, it should be as free as possible of local distortion (non-uniformity errors) in both the horizontal and vertical directions. We have framed these constraints in terms of the following requirements on the reference maps:

1. The reference map shall be a seamless and gap-free map pair consisting of a DEM and a precisely co-registered appearance map centered at the landing site.
2. The reference map shall have a bounded angular error around the normal to the map tangent plane at the center of the map. The specific error bound will be dictated by the TRN approach.
3. The reference map shall have a distortion (pixel to pixel knowledge error) of less than TBD m (99%) for distances less than TBD m between pixels and TBD m (99%) for all greater distances within the map footprint. The TBDs are a function of available orbital data and TRN requirements.

4. The reference map shall be constructed to match as closely as possible the lighting conditions present during landing.

For polar landing, low sun elevation and varying solar azimuth mean that orbital image data varies widely in appearance. As a result, the ideal image appearance map will need to be rendered from a DEM and an albedo map where available. In addition, shadows cast by neighboring terrain into the region of the reference map require that the map be much larger (have wider context) than strictly required by the TRN algorithm. We outline some additional considerations and challenges for polar landing:

1. Low sun elevation means that large regions are shadowed in overhead imagery. Lack of atmosphere and sky illumination means that these regions are completely dark. Use of multiple images taken at different sun and imager geometries may reduce but not eliminate the shadowed portions of a reference map.
2. Because the lunar satellites are in polar orbit, the imaging geometry is not ideal for standard photogrammetric methods. Camera pointing does not always result in a suitable stereo pair of images.
3. Appearance changes from small changes in sun angle result in much greater sensitivity in image matching algorithms. Thus, TRN algorithms become very sensitive to the timing at high latitude regions.

The LuNaMaps team has outlined a process for TRN DEM building as shown in Fig. 1. With team members at the Goddard Space Flight Center (GSFC), the Jet Propulsion Laboratory (JPL), and NASA Ames, we purposefully plan to have parallel pipelines for DEM building, DEM quality evaluation, and TRN performance evaluation in order to maximize our ability to eliminate potential sources of errors via cross-validation exercises as well as ensuring that the resulting map products are tested with at least two different TRN systems and lunar landing simulations.

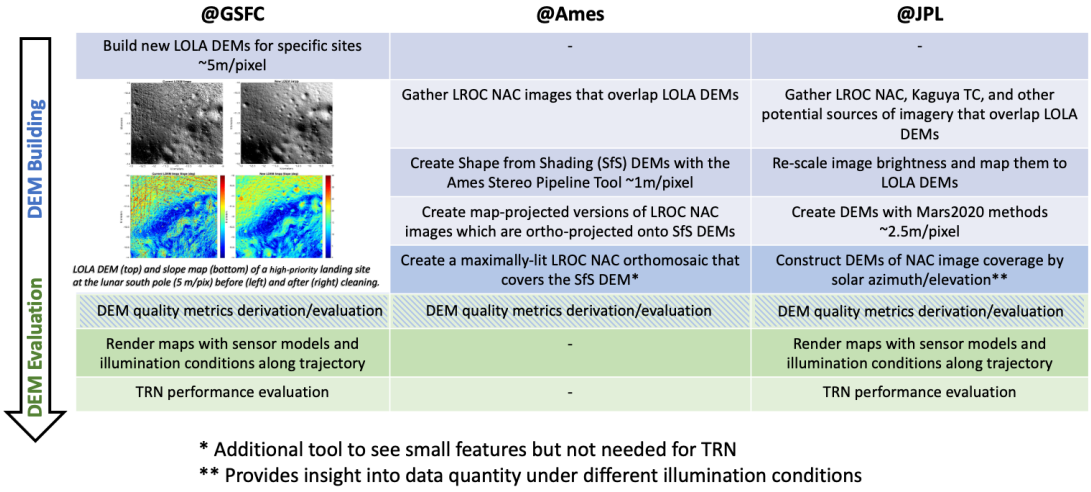

Fig. 1 TRN DEM Building Process

The process begins with a set of new and improved LOLA DEMs [10] for a specific lunar Region of Interest (RoI) with a resolution down to 5 meters/pixel. Subsequently, existing camera images that overlap the RoI are gathered, and a Shape from Shading (SfS) DEM is created using the Ames Stereo Pipeline tool [11], as well as other methods that will help cross-validate the final map products. The combination of LOLA DEMs and stereo images will yield higher-resolution map products of the RoI of approximately 1-2.5 meters/pixel. Larger map products of lower resolution are also needed to cover larger areas as viewed from higher altitudes given a trajectory leading up to the RoI. Existing data that are already publicly available may be sufficient for the higher altitude maps, however, these maps are also validated for use in TRN systems by decreasing all error sources that are relevant to spacecraft position estimates. The full set of benchmark maps for a given landing site will undergo a validation process to derive standard metrics, assess map quality, and identify the impacts of any significant map errors on navigation performance.

A. Enhancement Process for LOLA DEMs

Small errors in the LRO orbit reconstruction, typically about 7/7/0.5 m in the along-track/cross-track/radial directions [5], can cause streaky artifacts in a LOLA DEM (LDEM). Isolated noise returns (~1% of total) can appear as spurious "flag-poles" or "pot-holes". These artifacts become more apparent at higher DEM resolution (pixel scales less than ~20 m/pix) and can pose a challenge to TRN and detailed landing site studies. Most of these artifacts can be removed by adjusting the LOLA tracks to a reference DEM, such as those produced by stereo or SfS methods applied to LRO Narrow Angle Camera (NAC) images [12]. Due to gaps between tracks and individual laser spots, a 5 m/pix LDEM has a fill factor of only ~10% near the south pole (i.e., roughly 10% of 5 m pixels have data while the rest are interpolated). However, it still contains enough information to act as the reference DEM allowing this track adjustment process to produce a vastly cleaner LDEM with fewer artifacts. Updating the 5 m/pix LDEM in this way yields a product that is more useful for TRN, landing site studies, and as a constraint to higher-resolution DEMs from stereo and SfS. A major advantage of this process is that it enables realistic estimates of LDEM height uncertainties due to range error, orbital errors, interpolation, and sub-pixel sampling. Here we provide a brief summary of this process and refer the reader to Ref. [10] for additional details.

Our method for updating the LDEMs is based on an iterative process of fitting geolocated LOLA tracks to each other. We randomly remove 2% of the tracks from the 5 m/pix LDEM, adjust each of the missing tracks individually to the resulting "reduced" LDEM by applying 3-dimensional offsets and minimizing the root-mean-squared (RMS) surface height residuals between each individual laser return (referred to here as a point) and the surface height at that location on the current reduced LDEM. This step is repeated until all tracks have been adjusted. Fitting each track to a reduced LDEM with that track removed ensures that outliers can be detected and that the track is not adjusted to itself. Only nadir-pointing tracks are included since this process would not work as well for off-nadir tracks due to topographic visibility effects. The process of running 50 batches until all tracks are adjusted is repeated 5 times in total (yielding 250 total batches), each time starting from a new LDEM computed with the best-fit track adjustments from the previous iteration. Outlying points are down-weighted during the track fitting to ensure they do not bias the results, and are removed after the final iteration. The typical residual between each individual laser return and the reduced LDEM is about half a meter. The track adjustments (or offsets) at each iteration converge towards zero and their dispersion decreases. After 5 iterations, the typical track offsets are ~10-20 cm horizontally and a few cm vertically. Thus, the final geolocation uncertainty has been reduced by more than an order of magnitude over the original geolocation uncertainties. This geolocation uncertainty applies to total absolute position rather than the uncertainty in surface height, i.e., elevation above the reference sphere. Natural terrain slope and roughness variations and sub-pixel sampling cause the uncertainty in gridded surface height to be larger than the track geolocation uncertainty. After the final iteration, visual inspection of the hillshaded LDEM reveals a small percentage of isolated invalid LOLA returns (e.g., flag poles) and runs (streaks) of a few consecutive poor-quality returns. These points are identified and removed in an automated fashion according to two criteria: (1) high slope and (2) runs of large residuals. In total, of order ~0.1% of all points are removed by this last step. Fig. 2 shows a close-up of an example LDEM comparing the old version (left column) and the new version (right column). The hillshade (top row) and slope map (bottom row) show how the track adjustment and cleaning process have removed the vast majority of streaky artifacts and bad points. The largest improvements occur over regions of high slope since a constant horizontal geolocation error can translate to a larger vertical error in surface height as slope increases.

Detailed TRN and landing site studies may require knowledge of the spatially varying LDEM height errors. Instead of calculating the full error-covariance matrix of the LDEM, which would be computationally prohibitive, we create an ensemble of random realizations of the errors. Such a Monte Carlo approach is analogous to that used in the analysis of the Gravity and Interior Laboratory (GRAIL) lunar gravity field [13]. The LDEM errors can be considered to have a data component, due to orbital errors and interpolation, and a geologic component, due to natural terrain variations. We can take advantage of the self-similarity of lunar topography to generate simulated terrains with approximately the same statistical properties as the real terrain. In total, 100 such clones are generated for each site. These form a statistical ensemble with approximately the same error properties as the data. The clones allow us to explore the effects of orbital error and interpolation uncertainties on surface height without having to compute the full error-covariance matrix of the entire LDEM. We find that interpolation error is controlled primarily by gap size because larger gaps can accommodate larger height variations.

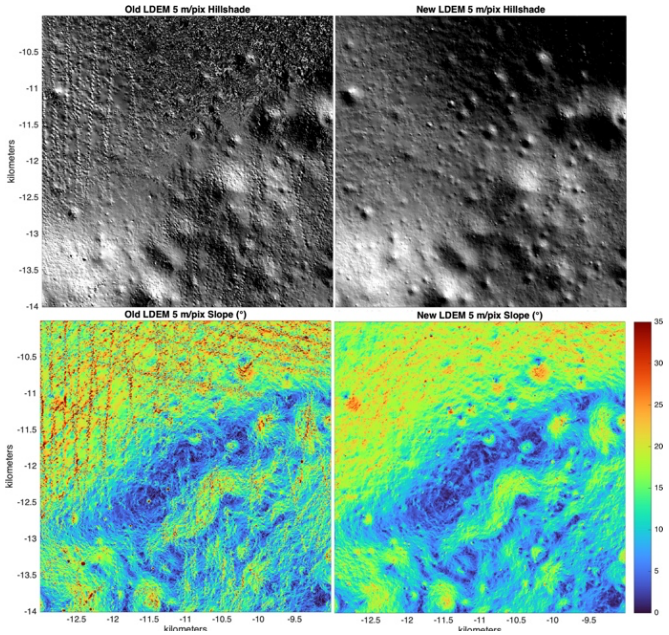

Fig. 2 Comparison between the old 5 m/pix LDEM (left column) and the new LDEM (right column). The hillshade (top row) and slope map (bottom row) show how the track adjustment and cleaning process has removed the vast majority of streaky artifacts and bad points.

In a recent study [10], we described these methods in more detail and applied them to 4 south pole locations previously identified as good potential landing sites based on their favorable illumination conditions [14]. For LuNaMaps, we are expanding the number of locations (Fig. 3) to other sites of interest and over greater areas to facilitate TRN studies. These new products will be made available to the community as they are completed at https://pgda.gsfc.nasa.gov/products/78.

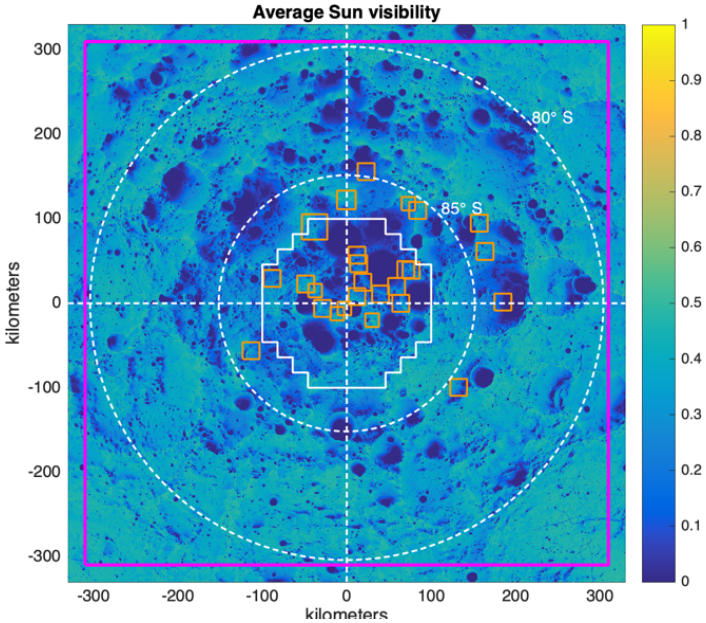

Fig. 3 Average illumination fraction of the Sun at the lunar south pole over a full 18.6 year precession cycle. Small orange squares and solid white lines (87-90° S) outline regions for which we are producing new 5 m/pix LDEMs. The large magenta box (80-90° S) outlines the region that will have a new 20 m/pix LDEM.

B. Shape from Shading DEMs

Stereo terrain models produce terrain that have a ground scale distance (GSD) that is some multiplier of the contributing input images. Such products are typically produced at three times the GSD of the poorest resolution of the pair (e.g. producing 3 m/pix DEMs from 1 m/pixel images) but the true information density could be worse. Additionally, due to the polar nature of the orbital and lighting geometries, stereo coverage of large areas is sometimes practically difficult. Photoclinometry or SfS can provide terrain models not at some multiplier of the original image GSD but approaching the length scales of those original images, providing a potentially better-resolved terrain model. Additionally, SfS does not require rigid stereo geometries, but benefits from many images with a wide variety of illumination conditions. The lunar poles provide a variety of solar illumination directions (azimuths), but a limited range of incidence angles. However, these conditions allow production of terrain models with GSDs approaching 1 m/pix [11], but the areas to which these techniques can be applied are limited to those which are illuminated.

C. Reference Map Construction at JPL

An alternative DEM building process from the LDEM/SfS approach described previously is also being developed at JPL. The JPL team learned a great deal from Mars 20202 Lander Vision System (LVS) reference map construction [15]. The Mars 2020 Perseverance rover landed within 5 m of the target selected by the safe landing system based on the fidelity of the LVS reference map developed by JPL team. Lessons learned from Mars 2020 will be applied to lunar reference map construction. We outline some important points:

1. Identify all possible error sources related to the final map product. Those error sources include camera intrinsic and extrinsic model error, ancillary data error including position and pointing error, image time tag offset, etc.
2. Remove or mitigate errors: Some of the errors such as the camera model and instrument timing error are well understood. We developed methods to remove or correct them. Other types of errors, such as image jitter, are more difficult to characterize. For these, we developed mitigation strategies to reduce impact and remain within LVS requirements.
3. Choose the best input data: We took into account multiple criteria in choosing the best data. The quality factors considered include image coverage, viewing angle, atmospheric opacity, image quality, and orbit determination solution accuracy. Where multiple options were available for ancillary data such as SPICE kernels and Mars orientation models, we determined the best options for our needs. Most of these considerations will apply to lunar reference maps.
4. Create two independent maps of the same site: For Jezero Crater, two LVS map were made from two independent CTX image sets. Comparison of the two independent maps was expected to reveal errors in processing or input data. Additionally, two maps were created by each of two teams, the JPL team and the USGS Astrogeology Science Center team, using different tools and procedures. The comparison of the two sets of maps from identical input data and different procedures was expected to reveal procedural or other errors in either approach. We plan to approach validation of lunar reference maps in the same way: data cross validation and cross-organizational validation.

Preliminary work at JPL has focused on data gathering and validation and data source characterization. A few early findings follow.

LOLA SPK is more consistent than LROC SPK: There are two LROC trajectory kernels, LROC SPK and LOLA SPK. We use ray gap (the minimum distance between rays corresponding to matched points in a stereo pair) as an indirect measure of accuracy. Using the two available SPK kernels, with all other data kept constant, we find that the LOLA SPK product results in a consistently better estimate (Fig. 4).

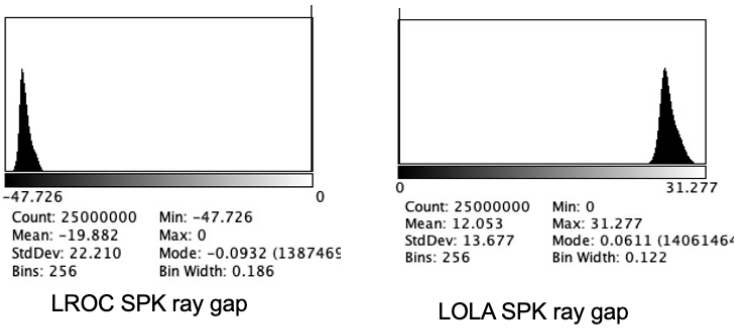

Fig. 4 Error in intersection between rays from corresponding pixels (ray gap error) in NAC stereo pair using LROC position kernel (left) and LOLA position kernel (right) with identical attitude information. The uncorrected LOLA kernel has systematically lower error.

The LROC NAC time tag has a time offset from the SPICE time tag. During Mars 2020 LVS reference map construction, we found that the CTX camera time tag is not perfectly synchronized with the MRO clock. Because LROC NAC is a similar camera, we considered whether a similar issue existed. A set of NAC images over one target site was selected for this study. We found that applying a small timing correction to the NAC images significantly reduced ray gap errors (Fig. 5). Like MRO CTX camera, similar time off set was found in LROC NAC image. The magnitude of error caused by time offset can be as much as 100 meters. A simple offset compensation reduces the error to single meter level.

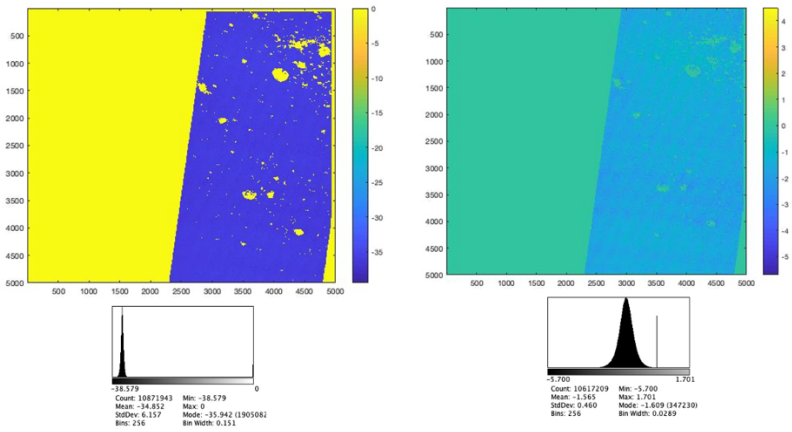

Fig. 5 Result of introduction timing correction to NAC stereo pair. Uncorrected ray gap error (left) is an order of magnitude larger than the time corrected ray gap error (right).

The LROC NAC camera model contains ~2 pixels radial distortion error. After a time offset correction, the correlation map between two orthorectified NAC images (M109197379LC M1106040240LC) with similar flight path shows some remaining distortion (~2 pixels) in the NAC camera model, which may be uncompensated radial distortion. The disparity map between two orthorectified NAC images, which have similar flight path, shows some likely radial distortion (Fig. 6).

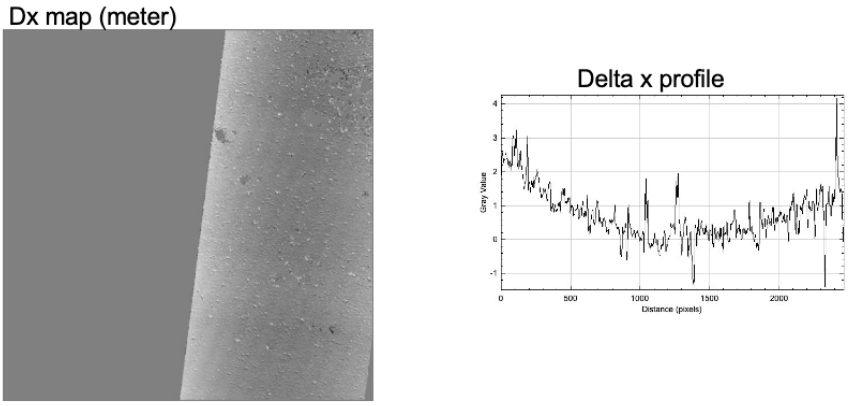

Fig. 6 Disparity map between NAC stereo pair in direction orthogonal to spacecraft motion (left). Profile of single scanline (right). Observed pattern is consistent with uncorrected radial distortion.

The NAC camera extrinsic data has some residual orientation error. Two overlapping orthorectified NAC images, one southbound and one northbound are used for this study. The relative time offset between them was corrected first. Then the horizontal (dx) and vertical (dy) disparity maps between them are extracted. The disparity maps show an S-curve displacement perpendicular to the flight direction. This is consistent with an orientation error. The delta x and y maps between the southbound and northbound NAC image shows S curve displacement. This displacement is likely caused by camera extrinsic attitude error (Fig. 7).

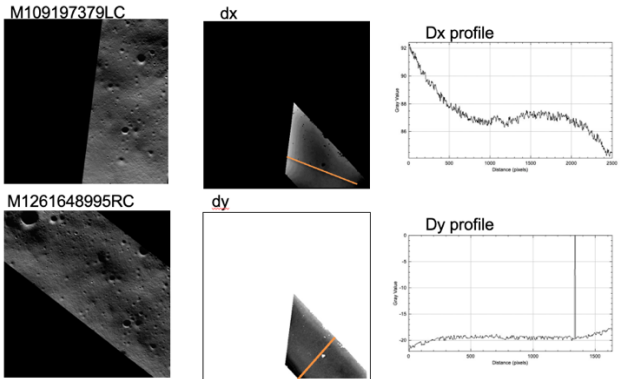

Fig. NAC stereo pair (left), disparity field in direction across (center, top) and along (center, bottom) spacecraft motion. Disparity along orange lines shown in detail on right. Disparity pattern is consistent with error in rotation knowledge.

IV. Hazard Detection Map Products

A separate benchmark data set of higher-resolution map products will be produced for the purpose of supporting the development and testing of HD systems. Starting with the highest-resolution TRN DEMs, small cm-scale surface features (e.g., small rocks and craters) will be added to the maps to generate representative map products of different types of lunar regions (i.e. different types of geological features). These high-resolution map products will not match the reality of any specific site since there are very few locations on the lunar surface that have been imaged at cm-scale resolution. However, they will have properties qualitatively and quantitatively consistent with our current geological understanding of the surface. There are two possible methods for enhancing the resolution of the TRN DEMs that are derived from orbital imagery to increase their resolution to cm-scale, Lunar-analog field data and synthetic lunar features. The LuNaMaps project will evaluate both methods and provide a final benchmark data set to be shared with the community. The current plan for building the HD benchmark map products is shown in Fig. 8.

Similar to the process for building the TRN map products, the LuNaMaps team plans to have parallel processes to leverage our ability to validate and test the DEMs with separate software tools. Field geologists from GSFC are collecting relevant lunar-analog field data that will be used to extract a catalog of lunar surface features that can then be used to synthetically enhance the TRN DEMs to where they are cm-scale resolution and representative of different types of lunar regions. Additionally, the team currently plans to leverage an existing high-end lunar simulation environment software that has been designed for the VIPER rover [16], to incorporate geological features from the catalog into the TRN DEMs to increase their resolution so they can be used for HD simulations.

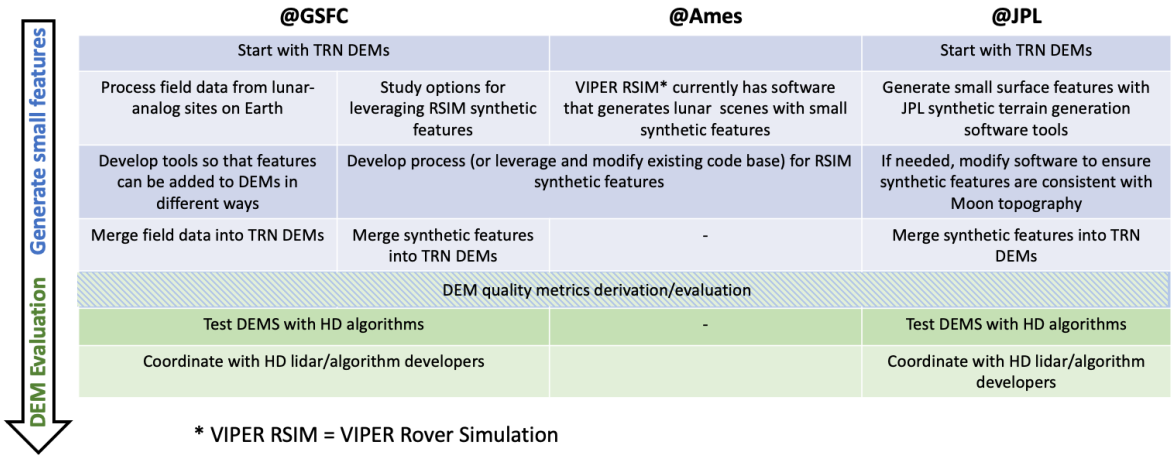

Fig. 7 Enhanced Hazard Detection DEM Building Process

A. Lunar-analog Field Data

The first method is to collect field data at lunar-analog sites on Earth using lidar or camera-based surveys of relevant terrain and develop the methodology to process the field data, categorize it into types of lunar regions, and merge it into the TRN DEMs. The benefits of this method are that the data will be based on real features, and will contain realistic errors and noise from the instruments used to collect it. Consequently, the enhanced DEM will be more realistic for HD simulations and especially HD algorithms that need to be robust to noise when detecting and identifying surface hazards.

Lunar analog field surfaces have been identified in central Iceland and lidar and photographic data have been collected to generate elevation models of regions of interest for integration into synthetic TRN DEMs. Figure 9 shows one example site, which was last significantly modified during a small volcanic eruption in 1961. This site has meter to decimeter scale rocks protruding from a smooth blanket of millimeter and smaller-grained basaltic regolith. An elevation model and orthomosaic has been generated using stereophotogrammetry with small Uncrewed Aerial Systems (sUAS) photographs. These raster products are <5 cm in spatial resolution and contain features relevant to TRN simulations including smooth areas, clusters of boulders, and isolated blocks. Some individual sites, including Fig. 9, are much rockier than expected for lunar landing sites, though these surfaces can test end-member scenarios for TRN simulations.

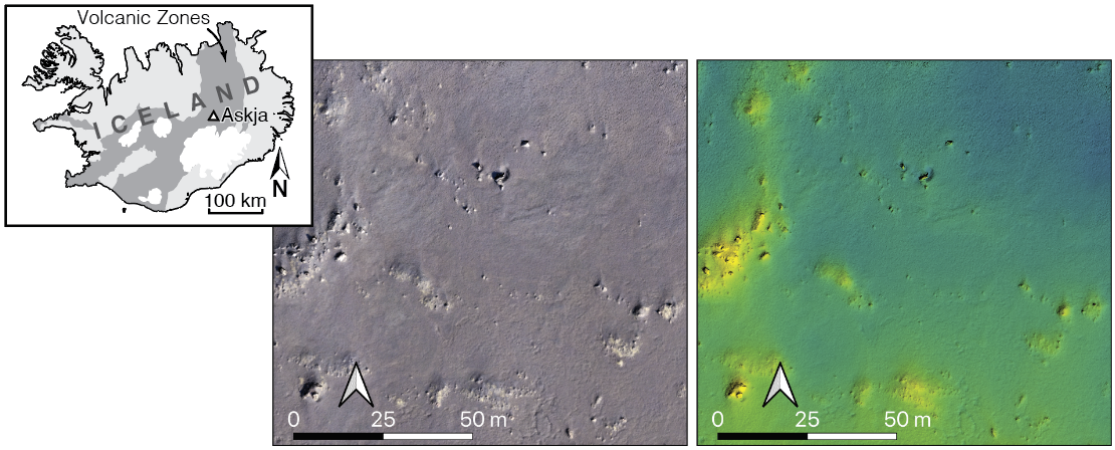

Fig. 8 One example field analog landscape at the Askja Volcano, Iceland. Center: a 1 cm orthomosaic is generated of a location with isolated and clustered rocks on a sheet of sand and silt-sized regolith. Right: a 3 cm digital elevation map has also been generated at this site. Note the colors represent a total elevation relief of <3m (blues are ~997 meters above sea level, yellows are 1000masl)

B. Synthetic Lunar Surface Features

A second method for adding small hazards will be to synthetically generate them with software and merge the data into the TRN DEMs. The advantage of this method is that it offers more control over hazard shapes and sizes, and their spatial distribution. This can be done in different ways depending on the constraints of the software or processor being tested.

Photographs of individual rocks are also taken at field sites of interest, including Iceland, for integration into synthetic lunar surface terrains. These photographs are used to generate shape models of each individual rock, essentially building a library of rock hazard objects. These objects in the field vary from angular to sub-rounded clasts, 10 cm in length to over 1 m (Fig. 10). Rocks included in this catalog will predominantly be of volcanic origin, including mafic and felsic compositions at different lunar analog field sites.

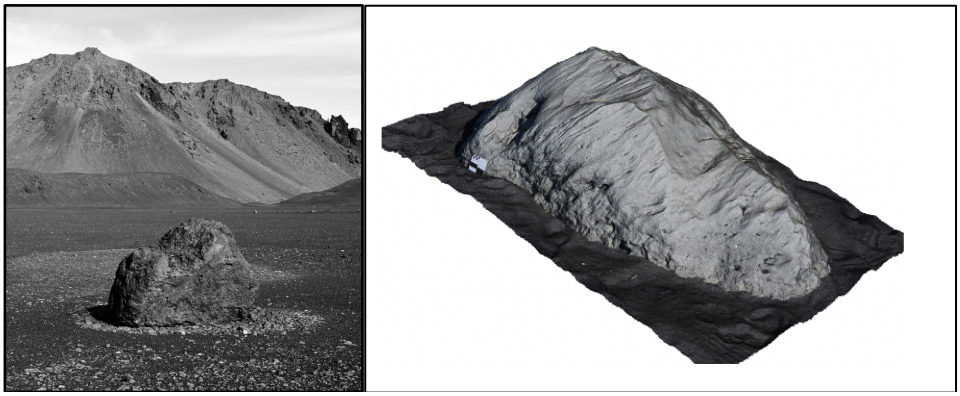

Fig. 9 Examples of rocks to be integrated into synthetic DEMs as potential landing hazards. Left: a single sub-rounded boulder at the same field site has been photographed to create a 3D shape model (Photograph Credits: D. Pettit). Right: Example of a high-resolution basaltic rock model from the boulder field in northern Iceland rendered in 3D. The black and white scale bar against the rock is 10 cm.

V. Map Validation and Verification

Once the initial benchmark data sets have been generated, the project has the goal of developing processes for validating map products leveraging the lessons learned from both Mars2020 and OSIRIS-REx. Part of this process will consist of assessing different software pipelines, primarily one at GSFC and one at JPL, and comparing results between the separate sets of map products. This will allow the team to define map quality metrics and how to compute them, as well as to provide the community with a suggested set of guidelines in terms of what error types are most critical for TRN and HD systems.

Figure 11 shows a flow chart of the map validation and verification procedure being pursued by JPL. To validate a given reference map, we propose generating two maps from disjoint data sets. The consistency/inconsistency between the two maps will reveal potential errors from input data and models. At the same time, we will compare to maps generated using independent processing chains on identical data. The comparison is expected to reveal any systematic errors in approach or methodology in any of the processing chains. Finally, we will compare the reference maps with independently generated map products such as from Kaguya, Chang'e 2 or Chandrayaan.

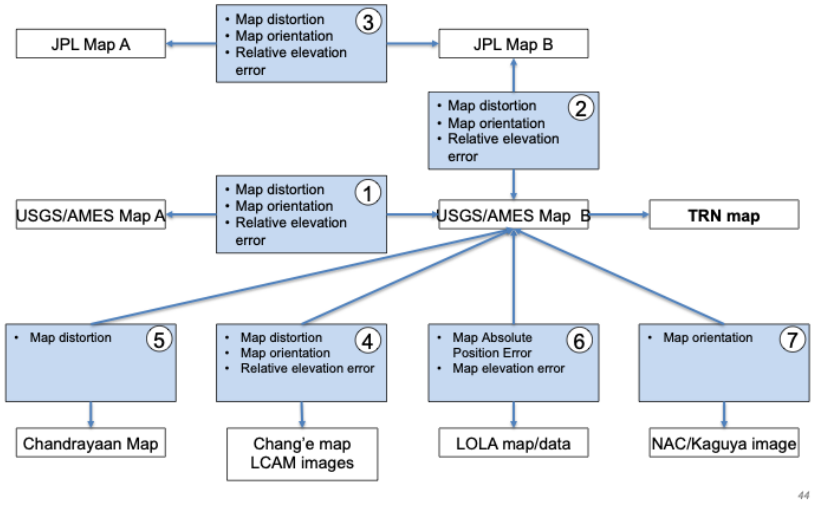

Fig. 10 Flowchart for Map V&V at JPL

Additional sensitivity analyses will be done by GSFC to study and quantify potential map errors. This will consist of direct comparison of generated maps to NAC images as shown in Fig. 12. Each map will be distorted by several different transformations to mimic potential errors in the DEM construction process. These deformations may be local (such as adjusting the height of a specific pixel on the DEM) or global (such as flattening or scaling the entire DEM). Once these deformations are applied, the DEM is rendered and compared with corresponding NAC images to identify differences. The deformations applied will be varied until the rendered image deviates from the image collected by NAC, at which point an upper-bound on the potential error can be identified.

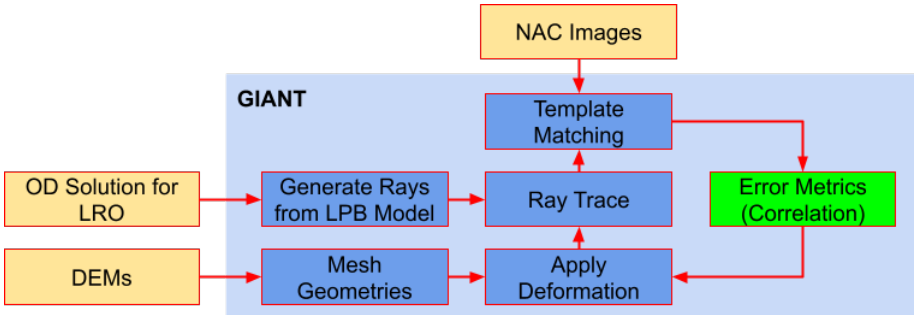

Fig. 11 Rendered DEM to NAC Image Comparison Flowchart

VI. TRN Performance Evaluation

Monte Carlo simulations will be used to evaluate navigation performance once a concrete set of DEM quality metrics has been identified based on the results from both the JPL and GSFC pipelines. Specifically, the goal is to determine how different types of errors in the DEMs impact the overall TRN performance.

The Goddard pipeline is depicted in Fig. 13. For a given reference trajectory, images and lidar measurements are simulated using the Goddard Image Analysis and Navigation Tool (GIANT) [17]. Due to the large size of all available lunar data sets, a pre-processing step is conducted where only the maps of the required resolution are considered, and the specific regions to load are identified. The rendering is done assuming a single bounce ray tracing algorithm treating the sun as point, while lidar is simulated considering only the light-time delay. Once a set of synthetic truth images have been created, a Monte Carlo analysis is run where each DEM used for TRN is distorted by randomly sampling the error metrics previously determined, and a predicted template is rendered of this distorted DEM, and cross-correlation based image registration is performed using the onboard version of GIANT [18].

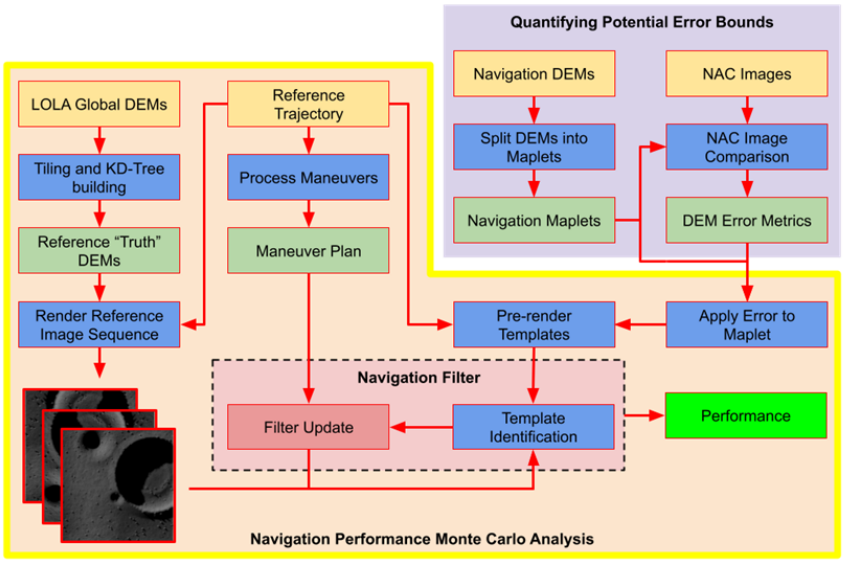

Fig. 12 TRN Performance Evaluation Pipeline at GSFC

For the image-to-map matching step (Fig. 14), two different methods of image registration for TRN will be considered: Image-on-Map, and Maps-on-Image. The Mars2020 approach was to match flight images to a larger reference map while the OSIRIS-Rex approach was to render small templates within the area seen by the larger camera field-of-view. Considering both approaches will allow us to ensure that methods developed here are as TRN-algorithm agnostic as possible.

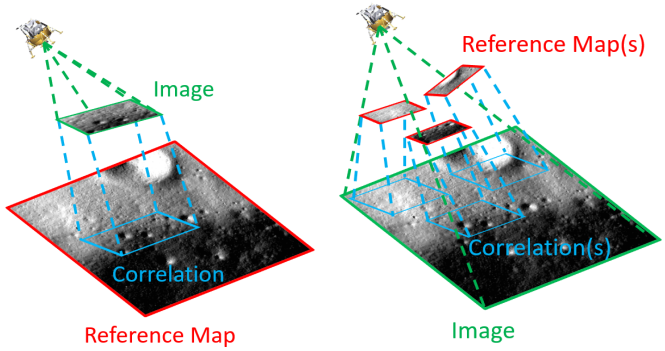

Fig. 13 Correlation between Images and a Reference Map

VII. Summary

TRN and HD have both been successfully performed autonomously on previous NASA missions, however, these missions spent significant effort developing unique TRN/HD algorithms, navigation maps, and validation pipelines. Given the interest in repeated landing at multiple Lunar locations in the near future, continuing the process of building everything from scratch will prove prohibitively expensive. Therefore, in the LuNaMaps project, we are seeking to address this issue by creating a set of validated navigation maps for Lunar sites of interest freely useable by anyone and a demonstrated robust validation pipeline for other navigation maps and HD algorithms, enabling upcoming missions to focus on TRN and HD algorithm and hardware development. In this paper we have described our current progress and anticipated next steps to make the community aware of this work and how the results can be acquired. We believe that the finished products will prove extremely valuable in making the Lunar surface more accessible to NASA and others going forward.

Acknowledgments

The authors would like to acknowledge Nikolas Trawny and Andrew Johnson at JPL, John Carson, Michelle Munk, Bo Naasz, Wade May, and Terry Fong at NASA HQ for their support on this work and all the help they provided to get this project started. A portion of this research was carried out at the Jet Propulsion Laboratory, California Institute of Technology, under a contract with the National Aeronautics and Space Administration.

References

[1] Sostaric, R. R., et al. "The SPLICE Project: Safe and Precise Landing Technology Development and Testing", *AIAA Scitech 2021 Forum*.

[2] Johnson, A. E., et al. "The Lander Vision System for Mars 2020 Entry Descent and Landing", *AAS Guidance and Control Conference, 2017*.

[3] Lorenz, D.A. et al., "Lessons Learned from OSIRIS-Rex Autonomous Navigation Using Natural Feature Tracking"

[4] Laura, J.R. and Beyer, R.A., "Knowledge Inventory of Foundational Data Products in Planetary Science", *The Planetary Science Journal (2021),* Volume 2, Number 1.

[5] Mazarico, E.; Neumann, Gregory A. ; Barker, Michael K. ; Goossens, Sander ; Smith, David E. ; Zuber, Maria T. (2018). "Orbit determination of the Lunar Reconnaissance Orbiter: Status after seven years". *Planetary and Space Science*, Volume 162, p. 2-19.

[6] Smith, D. E. et al. (2017). "Summary of the results from the lunar orbiter laser altimeter after seven years in lunar orbit". *Icarus*, Volume 283, p. 70-91.

[7] Robinson, M. S., et al., (2010), Lunar Reconnaissance Orbiter Camera (LROC) Instrument Overview, *Space Science Reviews, 150, 81-124.*

[8] Henriksen, M. R., et al., (2017), Extracting Accurate and Precise Topography from LROC Narrow Angle Camera Stereo Observations, *Icarus, 283, 122-137*

[9] Haruyama, J. Et al. "Lunar Global Digital Terrain Model Dataset Produced from SELENE (KAGUYA) Terrain Camera Stereo Observations", 43rd Lunar and Planetary Science Conference, 2012.

[10] Barker, M. K., "Improved LOLA Elevation Maps for South Pole Landing Sites: Error Estimates and their Impact on Illumination Conditions", *Planetary and Space Science (2020)*

[11] Beyer, Ross A., Alexandrov, Oleg, McMichael, Scott (2018). "The Ames Stereo Pipeline: NASA's Open Source Software for Deriving and Processing Terrain Data". Earth and Space Science. American Geophysical Union (AGU). 5 (9): 537–548.

[12] Gläser, P. ; Oberst, J. ; Neumann, G. A. ; Mazarico, E.; Speyerer, E. J. ; Robinson, M. S. (2018). "Illumination conditions at the lunar poles: Implications for future exploration". *Planetary and Space Science*, Volume 162, p. 170-178.

[13] Lemoine, Frank G. ; Goossens, Sander ; Sabaka, Terence J. ; Nicholas, Joseph B. ; Mazarico, Erwan search by orcid ; Rowlands, David D. ; Loomis, Bryant D. ; Chinn, Douglas S. ; Neumann, Gregory A. ; Smith, David E. ; Zuber, Maria T. (2014). "GRGM900C: A degree 900 lunar gravity model from GRAIL primary and extended mission data". *Geophysical Research Letters*, Volume 41, Issue 10, pp. 3382-3389.

[14] Mazarico, E. search by orcid ; Neumann, G. A. ; Smith, D. E. ; Zuber, M. T. ; Torrence, M. H. (2011). "Illumination conditions of the lunar polar regions using LOLA topography". *Icarus*, Volume 211, Issue 2, p. 1066-1081.
[15] Cheng, Yang, Ansar, A., Johnson, A.E., "Making an onboard Reference Map from MRO/CTX Imagery for Mars2020 Lander Vision System", August 2021 Earth and Space Science 8(8)
[16] M. Allan *et al*., "Planetary Rover Simulation for Lunar Exploration Missions," *2019 IEEE Aerospace Conference*, 2019, pp. 1-19, doi: 10.1109/AERO.2019.8741780.
[17] Liounis, A. J., et al. "Independent optical navigation processing for the OSIRIS-REx mission using the Goddard Image Analysis and Navigation Tool," 2nd Annual RPI Workshop on Image-Based Modeling and Navigation for Space Applications, Saratoga Springs, NY, 2019.
[18] Gnam, C. G., et al. "A Novel Surface Feature Navigation Algorithm Using Ray Tracing," 2nd Annual RPI Workshop on Image-Based Modeling and Navigation for Space Applications, Saratoga Springs, NY, 2019.